EVALUATION OF THE IMPACT OF A NEW QUALITY CONTROL METHOD ON ASSIMILATION OF CRIS DATA IN HWRF-GSI

Ding Liang[1], and Fuzhong Weng[2]

Affiliation: [1]IMSG, College Park, MD, USA
[2] NOAA, College Park, MD, USA

ABSTRACT

In this paper we evaluate the potential of assimilation of Cross-track Infrared Sounder (CrIS) radiance in the warm start HWRF system for Hurricane Sandy forecast using collocated Visible Infrared Imaging Radiometer Suite (VIIRS) cloud product for cloud detection and CrIS channels clearing. We examine the CrIS data bias correction and quality control procedure in GSI. Then we compare the cloud parameters retrieved from GSI stand-alone algorithm with those from CrIS/VIIRS collocated cloud products. And the impact of applying CrIS/VIIRS collocated cloud products on CrIS quality control in GSI has been evaluated.

***Index Terms*—** CrIS, VIIRS, quality control, data assimilation

1. INTRODUCTION

CrIS onboard Suomi National Polar-orbiting Partnership (Suomi NPP) that was launched in October 2011 is an advanced Michelson interferometer with dynamic alignment and automatic internal spectral calibration. It is descendant of AIRS on board Aqua satellite. It scans 30 earth scene fields-of-regard in a cross-track manner within +/-50 degrees from the nadir direction. Each field-of-regard consists of 9 fields-of-view in a 3x3 array. The size of FOV is 14 km at nadir. It has a total of 1305 channels with channels 1-713 fall into the long-wavelength infrared band (9.14 - 15.38 μm), channels 714-1142 fall into the mid-wavelength infrared band (5.71 - 8.26 μm) and channels 1143-1305 fall into the Short-wavelength infrared band (3.92 - 4.64 μm). The high spectral resolution and wavelength coverage of CrIS enable it to provide global coverage of atmospheric temperature and water vapor with high vertical resolution of 1-2km in the troposphere and 3-5km in the stratosphere [Han et. al. 2014]. Research shows that a subset of 399 channels can fully represent the 1305 channels in data assimilation [Gambacorta, A. et. al., 2012].

Infrared sounder radiance is very sensitive to cloud and currently radiative transfer model in GSI models radiance under clear sky conditions. It is important to determine the infrared sounder radiance that has been contaminated by cloud before assimilation them into the numerical weather prediction models. A stand-alone cloud detection algorithm based on minimum residual method to estimate cloud-top pressure and effective fractional cloud cover in infrared sounder FOVs from infrared sounder radiance has currently been applied in GSI [Eyre, J. R. et. al. 1989]. The cloud-top pressure is then used to detect cloud contamination to infrared sounder channels.

High spatial resolution imager data can be used to improve infrared sounder pixel cloud detection with spatially and temporally collocated imager products [Li et. al., 2004]. As MODIS has been used to improve cloud detection for AIRS pixels. VIIRS is being applied to improve cloud detection for CrIS. VIIRS on board SNPP is a whiskbroom scanning radiometer with a total FOR of 112.56 degree in the cross-track direction. It has a total of 22 channels with 16 moderate resolution M bands with spatial resolution of 750m x 250m at nadir, 5 imaging resolution I bands with spatial resolution of 375m x250m at nadir and 1 day-night band with spatial resolution of 750m throughout the scan. [Cao et. al. 2014]. Auxiliary information including VIIRS SDR data from 13 M bands and 4 I bands and ancillary data are processed together to create flags which indicate the cloud conditions above VIIRS moderate resolution pixels. VIIRS pixels are flagged as confidently cloudy, probably cloudy, and probably clear or confidently clear in VIIRS cloud mask (VCM) products. Cloud phase which include water, opaque ice, cirrus, overlap or mixed phase will also be determined for pixels that are categorized as confidently cloudy or probably cloudy [Hutchison, K. D. et. al., 2005]. VCM is used to generate other datasets, including cloud products, ocean surface products, and land surface products and so on.

2. THE CRIS/VIIRS COLLOCATED PRODUCT

For every CrIS FOV, we can find the VIIRS pixels that fall in it by searching the VIIRS geolocation dataset. The number of VIIRS pixels of M16 band within the center CrIS FOV of a FOR ranges from over 200 at nadir to near 1400 off nadir [Wang, L. et. al.]. We calculate cloud fraction of a CrIS FOV from the ratio of confidently cloudy VIIRS pixels inside the CrIS FOV and clear fraction of a CrIS FOV from

the ratio of confidently clear VIIRS pixels inside the CrIS FOV. Other cloud parameters like cloud top pressure, cloud type and cloud layering are also calculated from averaging VIIRS cloud EDR products that inside a CrIS FOV. These cloud parameters together with CrIS BUFR data make a new CrIS/VIIRS BUFR data that can be used in data assimilation in NCEP GSI system.

Cloud Optical Properties algorithm derives cloud optical thickness and cloud effective particle size for daytime water phase clouds, and cloud optical thickness, cloud particle size and cloud top temperature for all other conditions.

For daytime water phase clouds, an iterative retrieval is used to find the cloud top pressure that makes the prediction from a fast radiative transfer model best matches the band M15 brightness temperature. The fast radiative transfer model is fed with cloud optical thickness and particle size and atmospheric/ surface state and. Cloud top temperature and Height are then determined from interpolation using atmospheric profile assuming atmosphere is hydrostatically.

For other clouds (nighttime water phase clouds and ice phase clouds), cloud top pressure is retrieved from hypsometric equation after determining the cloud top height from vertical interpolation of cloud top temperature.

A backup algorithm will be applied if the required inputs are missing or degraded.

Only band M15 (10.763um) is used for the Window Infrared (IR) retrieval of the cloud top parameters unit for daytime water clouds.

3. DATA ASSIMILATION

3.1. Bias correction

GSI bias correction consists of three parts for CrIS observations of channel i at FOR j ($i = 1, \dots I; j = 1, \dots, 30$): air-mass dependent bias ($b_{i,j}^{(1)}$), scan angle dependent bias $b_{i,j}^{(2)}$ and variational radiance angle bias $b_{i,j}^{(3)}$:

$$b_{i,j}^{(3)}\ b_{i,j} = b_{i,j}^{(1)} + b_{i,j}^{(2)} + b_{i,j}^{(3)}$$

$$= \sum_{l=1}^{5} \omega_l \times p_{i,j,l} + \alpha_{i,j} + \sum_{m=1}^{M} \gamma_{i,j,m} (\beta_j)^m$$

$p_{i,j,l}$ ($l = 1, \dots 5$) and $\omega_l$are five air-mass bias correction predictors and their coefficients. β_j and $\gamma_{i,j,m}$ are scan angle and the polynomial coefficients for angle bias correction up to the order of M. $\alpha_{i,j}$ is static scan angle biases, values of $\omega_l$and $\alpha_{i,j}$ are provided by GSI input file. The variational radiance angle bias correction is not applied in HWRF for CrIS bias correction.

The five air-mass bias correction predictors are defined as follows:

$$p_{i,j,1} = 0.01$$

$$p_{i,j,2} = \frac{1}{10} \times \left(\frac{1}{cos\theta} - 1\right)^2 - 0.015$$

$$p_{i,j,3} = (cos\theta)^2 \times clw$$

$$p_{i,j,4} = (\Gamma_{i,j} - \overline{\Gamma}_i)^2$$

$$p_{i,j,5} = \Gamma_{i,j} - \overline{\Gamma}_i$$

θ is satellite zenith angle. clw =0 for non-microwave sensors. For channel i at FOR j, $\Gamma_{i,j}$ is the integration over all model levels of the lapse rate dT multiplied by the difference of vertically adjacent transmittance. $\overline{\Gamma}_i$ is the averaged $\Gamma_{i,j}$over all FORs for channel i. $\Gamma_{i,j}$ is calculated by

$$\Gamma_{i,j} = 0.01 \times \sum_{k=1}^{K-1} (\tau_i^{k+1} - \tau_i^k) \times \left(T_{temp,k-1} - T_{temp,k+1} \right)$$

where subscript k indicates the k th vertical level, K is the total number of model levels.

3.2. Quality control

The quality control for CrIS in GSI employs five parameters.

The weighting function W_i is defined as follows:

$$W_i = \frac{1}{e_i^2} \times f_\theta \times (1 - (1 - f_H) \times \tau_i^1) \times \tau_i^{top}$$

where $e_i$is the observation error of the i^{th}channel. τ_i^1 is the transmittance at the first layer for the i^{th}channel, τ_i^{top} is the transmittance at the model top for the i^{th}channel , $f_\theta$and f_H are defined as follows:

$$f_\theta = \begin{cases} 1 - (\lambda_i - 2000) \times \tau_i^1 \times \max(0, \cos(\theta)) \times \frac{1}{400} \\ \quad if\ \theta < 89, f_{sea} > 0 and\ 2400 \geq \lambda_i > 2000 \\ \quad 0\ if\ \ \theta < 89, \mathrm{f_{sea}} > 0 and\ \lambda_i > 2400 \\ \quad 1 \quad otherwise \end{cases}$$

$$f_H = \begin{cases} \left(\frac{2000}{H}\right)^4 & if\ H > 2000m \\ 1 & otherwise \end{cases}$$

where $\lambda_i$is the wavenumber of the i^{th}channel, θ is solar zenith angle, $H$is the terrain height, $\mathrm{f_{sea}}$ is the fraction covered with water.

Then fractional cloud amount and cloud top pressure are calculated based on [Eyre, J. R. et. al. 1989]. Firstly, assume cloud top over the CrIS observation FOR is at atmosphere layer k ($k = 1,2, \dots K$), the fractional cloud amount N_k is calculated as follows

$$N_k = \min\left(\max\left(\frac{Sum_{1,k}}{Sum_{2,k}}, 0\right), 1\right) \tag{1}$$

where

$$Sum_{1,k} = \begin{cases} \sum_{i=1}^{n} (T_{B,i}^{Obs} - T_{B,i}^{Sim} - b_{i,j}) \times \\ \sum_{kk=1}^{k-1} (T_{temp,k} - T_{temp,kk}) \cdot temp_{kk,i} \cdot W_i \\ \sum_{i=1}^{n} (T_{B,i}^{Obs} - T_{B,i}^{Sim} - b_{i,j}) \times \\ \left(T_{temp,k} - T_{surf}\right) \cdot ts_i \cdot W_i \qquad if\ k = 1 \end{cases} \tag{2}$$

$$Sum_{2,k} = \begin{cases} \sum_{i=1}^{n} \left[\sum_{kk=1}^{k-1} (T_{temp,k} - T_{temp,kk}) \cdot temp_{kk,i}\right]^2 \cdot W_i \\ \sum_{i=1}^{n} \left[(T_{temp,k} - T_{surf}) \cdot ts_i\right]^2 \cdot W_i \qquad if\ k = 1 \end{cases} \tag{3}$$

In equations (2) and (3), $T_{B,i}^{Obs}$ and $T_{B,i}^{Sim}$ are the ith channel CrIS observed and CRTM simulated brightness temperatures, respectively, $b_{i,j}$ is the bias correction term, $T_{temp,k}$is the atmosphere temperature at layer k, $temp_{k,i}$ is i^{th} channel temperature sensitivity at atmosphere layer k, $T_{surf}$is surface skin temperature, $ts_i$is i^{th} channel skin temperature sensitivity.

The value of N_k which gives the minimum of the summation in equation (4) and the corresponding value of k are chosen as the retrieved effective fractional cloud amount and cloud top height. Figure 1 is the flow chart of this algorithm.

$$Sum_{3,k} = \begin{cases} \sum_{i=1}^{n}[(T_{B,i}^{Obs} - T_{B,i}^{Sim} - b_i) - N_k \cdot \sum_{kk=1}^{k-1}(T_{temp,k} - T_{temp,kk}) \cdot temp_{kk,i}]^2 \cdot W_i \\ \sum_{i=1}^{n}[(T_{B,i}^{Obs} - T_{B,i}^{Sim} - b_i) - N_k \cdot (T_{temp,k} - T_{surf}) \cdot ts_i]^2 \cdot W_i \quad for\ k = 1 \end{cases} \tag{4}$$

Additional constrains can be applied. If no combination of $N_k$and k can make equation (4) less than equation (5), then the retrieved effective fractional cloud amount is considered to be zero. a in equation (5) is tunable and currently set to 0.75. The flow chart of the search algorithm is in Figure. 1

$$Sum_{3,max} = a \cdot \sum_{i=1}^{n}\left[(T_{B,i}^{Obs} - T_{B,i}^{Sim} - b_i)\right]^2 \cdot W_i \tag{5}$$

skin temperature sensitivity related parameter :

$$dts = \left|\frac{\sum_{i=1}^{n}(T_{B,i}^{Obs} - T_{B,i}^{Sim} - b_i) \times ts_i \times W_i}{\sum_{i=1}^{n} {ts_i}^2 \times W_i}\right|$$

The last parameter is the modified observation error factor$e_i^{'}$, which is defined as:

$$e_i^{'} = e_i \times \tau_i^{top} \times f_{tropic}$$

Where:

$$f_{tropic} = \begin{cases} 0.5 + |lat| \times 0.02, if\ lat \in [25S, 25N] \\ 1, otherwise \end{cases}$$

e_i is observation error of the ith channel. $\tau_i^{top}$is transmittance at the model top.

The quality control in HWRF consists of the following six tests:

(1) If CRTM returns an error flag, all data are rejected.

(2) If $e_i > 10^4$, all data are rejected.

(3) If solar zenith angle $\theta < 89$, all data over ocean with $\lambda > 2400$ are rejected.

(4) If $T_{B,i}^{Obs} > 1000$ or $T_{B,i}^{Obs} \leq 0$, all data are rejected.

(5) If cloud is detected with cloud top at atmosphere layer K from equations (1) to (5) and $\tau_i^K > 0.02$, all data are rejected. τ_i^K is transmittance at atmosphere layer K for the i^{th}channel.

(6) If $dts > 1$, and $|\min(dTf, dts) \times ts_i| > max\ (0.05 \times e_i, 0.02)$, all data are rejected. dTf is a surface type related parameter. The values of dTf are 3, 2, 4, 2, 4 for sea, land, ice, snow and others respectively. If $ts_i > 0.2$, all data over land are rejected. $ts_i$is i^{th} channel skin temperature sensitivity.

(7) If $\left|T_{B,i}^{Obs} - T_{B,i}^{Sim} - b_i\right| > min\ (3 \times e_i^{'}, e_i^{max})$, all data are rejected, where $e_i^{max}$is the maximum observation error of the i^{th}channel. Currently $e_i^{max}$is set to 2.

The first and 3rd QC tests remove outliers when model simulations greatly deviate from observations. The (2) and (4) identify bad observation. The (5) removes outliers under cloudy conditions. The (6) removes outliers associated with uncertainty in surface emissivity under clear –sky condition. The (7) removes outliers when model simulations greatly deviate from observations.

4. EXPERIMENT SETUP AND RESULTS ANALYSIS

Two numerical forecast experiments were carried out. In the first experiment, conventional data, GPS RO data, ASCAT surface wind data and CrIS data are assimilated. In the second experiment, CrIS data are replaced by the CrIS/VIIRS data so that collocated VIIRS cloud products are used in cloud detection instead of GSI stand-alone CrIS cloud detection. The assimilation is run on both the parent and intermediate domains of HWRF and at 0600UTC Oct. 26 2012 and 1800UTC Oct. 26 2012 with a +/- 1.5 hour assimilation window.

Fig. 2 shows scatter plot of CrIS FOV color coded by cloud top pressure (unit: hPa) with GOES imager as background at 0600 UTC Oct. 26, 2012. Cloud top pressure data are from GSI stand alone algorithm for the left figure and cloud top pressure from collocated VIIRS pixels cloud top pressure for the right figure. Fig. 3 left shows scatter plot of CrIS FOV color coded by cloud type with GOES imager as background at 0600 UTC Oct. 26, 2012. Each cloudy VIIRS pixel is assigned to one of five cloud types: stratus, alto cumulus/stratus, cumulus, cirrus, cirrocumulus. Cloud type which dominates the VIIRS pixels inside the CrIS FOV is chosen as CrIS FOV cloud type. Right shows cloud top pressure difference (VIIRS minus GSI stand alone) and cloud fraction difference (VIIRS minus GSI stand alone) for the CrIS FOVs in the left figure. We can see that for high cloud like cirrocumulus and cirrus, cloud top pressure from GSI is lower than cloud top pressure from VIIRS, indicate cloud height from GSI is higher than those from VIIRS. For cumulus and alto cumulus/stratus, cloud top pressure from GSI is higher than cloud top pressure from VIIRS, indicate cloud height from GSI is lower than those from VIIRS. Fig. 4 left shows old QC flags and right figure shows new QC flags after applying CrIS/VIIRS collocated cloud top pressure in the QC process. It clearly shows the new QC method is superior to the current QC by discriminating FOVs under clear sky conditions that are flagged wrong as cloudy FOVs by the current QC method.

5. FUTURE WORK

New cloud products at VIIRS pixel resolution from CLAVR-X will be evaluated.

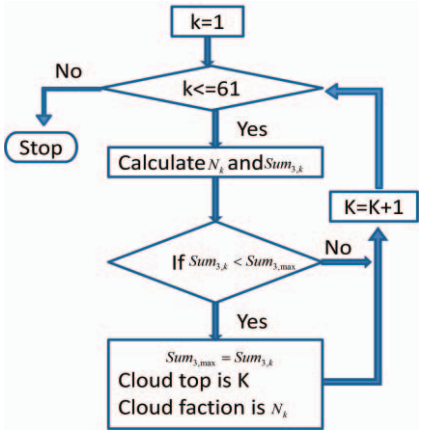

Figure 1. Flowchart for cloud top height and cloud fraction calculation

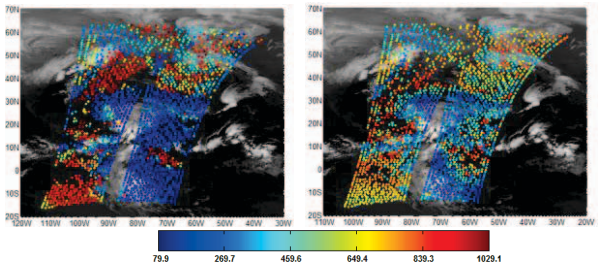

Figure 2. Scatter plot of CrIS FOV color coded by cloud top pressure (unit: hPa) with GOES imager as background at 0600 UTC Oct. 26, 2012. Left: cloud top pressure data are from GSI stand alone algorithm; Right: cloud top pressure from collocated VIIRS EDR cloud top pressure.

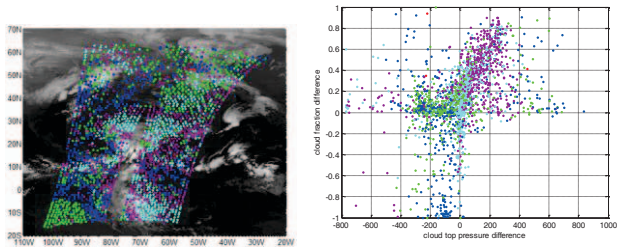

Figure 3. Left: Scatter plot of CrIS FOV color coded by cloud type with GOES imager as background at 0600 UTC Oct. 26, 2012. Each cloudy VIIRS pixel is assigned to one of five cloud types: stratus, alto cumulus/stratus, cumulus, cirrus, cirrocumulus. Cloud type which dominates the VIIRS pixels inside the CrIS FOV is chosen as CrIS FOV cloud type; Right: cloud top pressure difference (VIIRS minus GSI stand alone) and cloud fraction difference (VIIRS minus GSI stand alone) for the CrIS FOVs in the left figure.

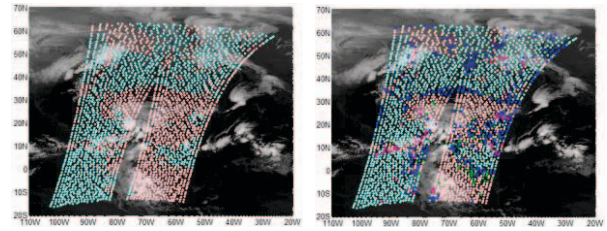

Figure 4. Left: Spatial distribution of CrIS channel 80 data points (699cm-1, 265hPa) passed all QC check (light blue) and failed through cloud check (light pink)
Right: Similar to the left figure, except: data points failed through old cloud check but passed all new QC check(blue) , passed all old QC check but failed through new cloud check (hot pink), failed through old cloud check but passed new cloud check and failed gross check (green). Both left and right figure are overlapped on GOES-13 brightness temperature at 0600 UTC Oct. 26, 2012.

11. REFERENCES

[1] Han, Y., et al. (2013), "Suomi NPP CrIS measurements, sensor data record algorithm, calibration and validation activities, and record data quality", *J. Geophys. Res. Atmos*., vol.118, Issue 22, pp. 12,734-12,748.

[2] Gambacorta, A. and Barnet, C.D. (2012), "Methodology and Information Content of the NOAA NESDIS Operational Channel Selection for the Cross-Track Infrared Sounder (CrIS)", *Geoscience and Remote Sensing, IEEE Transactions on* , Vol. 51 , Issue 6.

[3] Eyre, Jonathan R., W. Paul Menzel (1989), "Retrieval of Cloud Parameters from Satellite Sounder Data: A Simulation Study", *J. Appl. Meteor.*, vol. 28, pp. 267–275.

[4] Li, J., et al. (2004), "AIRS Subpixel Cloud Characterization Using MODIS Cloud Products", *J. Appl. Meteor.*, vol. 43, pp. 1083–1094.

[5] Cao, C., et al. (2013), "Suomi NPP VIIRS sensor data record verification, validation, and long-term performance monitoring", *J. Geophys. Res. Atmos.*, vol. 118, Issue 20, pp. 11,664-11,678.

[6] Hutchison, K.D., et. al. (2005), "Automated Cloud Detection and Typing of Data Collected by the Visible Infrared Imager Radiometer Suite (VIIRS)," *International Journal of Remote Sensing*, vol. 20, pp. 4681 - 4706.

[7] Wang, L., Y. Han, D. Tremblay, F. Weng and M. Goldberg, 2012, " Inter-comparison of NPP/CrIS radiances with VIIRS, AIRS, and IASI: a post-launch calibration assessment ", *Proc. SPIE 8528, Earth Observing Missions and Sensors: Development, Implementation, and Characterization II*, 85280J